Politecnico di Torino
Université de Paris
Laboratoire de Physique de l'École Normale Superiéure

Wideband and coherent detection with mid-infrared optical combs

Presented by LIVIA DEL BALZO

Double Degree Master Thesis in
Nanotechnologies and Quantum Devices

June 2021

Prof. Angela Vasanelli	Internship supervisor
Prof. Carlo Sirtori	Internship supervisor
Dr. Djamal Gacemi	Internship supervisor
Prof. Maria Luisa Della Rocca	Academic supervisor
Prof. Carlo Ricciardi	Academic supervisor

Contents

Introduction

This thesis contains the results of my internship at *Laboratoire de Physique de l'École Normale Superiéure*, done with *Quantum Devices* group (*QUAD*). The team research exploits the concepts of quantum mechanics, dealing in particular with light-matter interaction, to conceive new opto-electronic devices and systems in the mid and far infrared.
My work focuses on the study of quantum devices operating in the mid-infrared range, in particular at $9\mu m$ wavelength. This range of radiation is of great interest for techniques such as thermal imaging and spectroscopy [1], but also free space communication [2] and remote sensing [3]: finding good detection methods at this wavelength is thus extremely important. To this purpose, the report starts with a brief introduction on photonic detectors, their issues and figures of merit, after which my personal contribution is presented. During mu internship I had the opportunity to work with a new, unique, ultra stable Frequency Comb laser. In the first part of my internship I used the frequency comb to perform the characterization in time and frequency domain of a room temperature Quantum Cascade Detector (QCD) fabricated by one member of the team; then I performed the active stabilization of a Distributed Feedback (DFB) Quantum Cascade Laser (QCL) on the Frequency Comb. Note that an important part of my work was devoted to setting up these two experiments from scratch,finding good alignment conditions and learning to work with mid-infrared optics. Being able to have a stable QCL is a fundamental step towards the study of ultra-sensitive heterodyne detection for remote sensing, i.e. for the realization of LIDAR experiments in the mid-infrared range.

Part I

Context of the internship

Chapter 1

Mid-Infrared Detection

1.1 MIR electromagnetic radiation

Within the infrared range of electromagnetic radiation, spanning between the wavelengths of $700nm$ and $1mm$, the mid-infrared (MIR) region is defined as the interval between $3\mu m$ and $50\mu m$. In particular, the spectral band $8 - 14\mu m$ is of great interest for sensing technology: gas sensing and molecular spectroscopy are important applications of mid-infrared detection, due to the fact that a large number of molecules undergo strong vibrational transitions in this range of wavelengths. In addition to that, the earth atmosphere is almost transparent at these frequencies, so that many experiments in the field of thermal imaging, free space communication or remote sensing are feasible without absorption losses from the atmosphere. Despite these benefits, any object at T = 300 K emits black-body radiation in this range, constituting a source of background noise for MIR detectors: in the design of a good detector it's thus important to discriminate between the real signal and the unwanted one. The wavelength at which my experiments have been performed is $9\mu m$, corresponding to a photon energy of approximately $140meV$. This energy is not far from room temperature thermal energy ($k_bT = 26meV$) that can provide a further source of unwanted signal (Johnson noise) : minimizing this noise is another important issue concerning mid-infrared detectors.

1.2 Photonic detectors

Among IR detectors we focus on photodetectors, in which the optical radiation is absorbed inducing an electronic transition. The optical signal is then converted into an electrical signal easily measurable (as current in photoconductive or voltage in photovoltaic devices). Depending on the nature of electronic transitions in light-matter interaction we distinguish between

- Interband photodetectors: they exploit electronic transitions between valence and conduction band of the semiconducting material employed. In the mid-infrared, one

of the most widely used interband detector is HgCdTe due to its small energy gap. In my internship, I have been using one of these detectors, VIGO 83998, operating at room temperature.

- Intersubband photodetectors: they are based on electronic transitions inside the conduction band of heterojunctions, occurring between different subbands in a quantum well where electrons are confined (intersubband transitions).

The last category represents a great innovation since we deal with unipolar devices, not subject to electron-hole recombination between conduction and valence band which is responsible for the limited response time and frequency bandwidth of interband devices. Moreover, intersubband detectors are based on multi-quantum well structures which allow more degrees of freedom in band structure engineering, like modifying the size of the wells and the height of the barrier to tune the resonance frequencies and carrier lifetime. Quantum well infrared photodetectors (QWIP [4]) and quantum cascade detectors (QCD [5]) are the result of band engineering to achieve optimal absorption of light and good electronic transport properties at the same time. In figure 1.1 I report schematically a QWIP and QCD band structure: the QWIP structure is biased and a dark current is superimposed to the photocurrent, while in the QCD the photocurrent can be extracted without bias using the asymmetry of the potential formed by the tunnel coupled quantum wells, so the contribution of the dark current is practically negligible. During my internship I have characterized the frequency response of a quantum cascade detector.

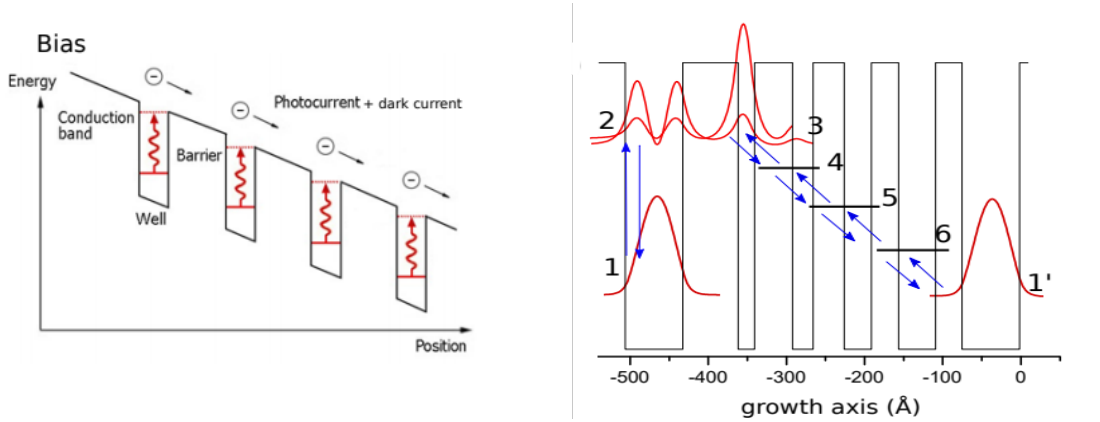

(a) QWIP band structure: increasing the number of wells the photon absorption increases at the cost of reducing the photoconductive gain i.e. the number of photoexcited electrons being transported along the circuit [4]

(b) QCD band structure: electron excitation (photon absorption) occurs at steps 1-2, the electron-phonon scattering cascade (responsible for electron extraction) occurs at steps 3 to 6 while 1' represents the active well of the next period. [6]

Figure 1.1

It is important to mention that intersubband transitions obey peculiar polarization selection rules derived from the Fermi Golden Rule for light matter interaction:in this kind of transitions, in fact, only the light polarized along the heterojunction growth direction can be absorbed and thus interact with the quantum well. Figure 1.2 shows a typical light

coupling geometry with a 45° polished edge facet, which allows one to have a component of the electric field along the growth direction and thus maximize absorption.

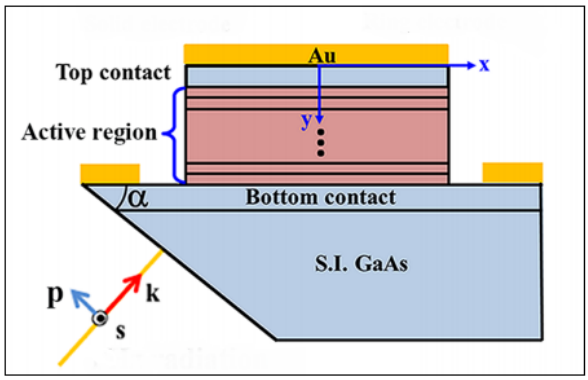

Figure 1.2: Sketch of a 'mesa' geometry with its 45° facet. Adapted from [7]

1.2.1 Figures of merit

In order to compare the performances of different detectors it's important to know some figures of merit, the most important being listed below [8]:

- **Responsivity**
  Capability of the device of converting the impinging optical signal into an electrical one, it's given by the ratio between the photocurrent and the incident power.

$$\mathcal{R} = \frac{I_{phot}}{P_{in}} [\,\mathrm{A/W}] \tag{1.1}$$

- **Noise Equivalent Power**
  Connected to the previous quantity, it describes the minimum optical power that can be detected by the device in the resolution bandwidth

$$NEP = \frac{\text{Current noise}}{\text{Responsivity}} = \frac{i_n}{\mathcal{R}} \quad \left[\,\mathrm{W}/\left(\mathrm{Hz}^{1/2}\right)\right] \tag{1.2}$$

- **Detectivity**
  It's the inverse of the NEP normalized by the detector area

$$D^* = \frac{\sqrt{A}}{\mathrm{NEP}} = \frac{\mathcal{R}\sqrt{A}}{i_n} \tag{1.3}$$

- **Frequency response**
  Responsivity of the photodetector in the frequency domain

$$R(\lambda)_\mathrm{f} = \frac{R(\lambda)_0}{\sqrt{1 + (2\pi f \tau_c)^2}} \tag{1.4}$$

where $R(\lambda)_0$ is the direct current low frequency responsivity, and τ_c is the response time, related to the cut-off or 3 dB bandwidth f_c as $f_c = 1/(2\pi\tau_c)$. The response time, or temporal resolution, gives an idea of how fast the detector response is to an instantaneous change of the optical signal, and depends on the carriers lifetime inside the photodetector. In an intersubband device the typical excited state lifetime is approximately 1 ps which corresponds to a cut off frequency of 160 GHz [9].

1.3 Heterodyne detection

This paragraph describes the principle of heterodyne detection, a peculiar technique that aims at increasing the sensitivity of a detection system and that I exploited for my experiments. In an heterodyne setup a signal at a certain frequency is combined with another signal, much more powerful, called 'local oscillator' (LO) at a slightly different frequency. A power-law detector's response (like the QCD or the VIGO) is proportional to the square of the electric field so that, assuming signal and LO have linearly polarized fields, their combination is given by the following formula [10]

$$\begin{aligned} &E_h(t)^2 = \left[E_S \cos\left(\omega_S t + \phi_S\right) + E_{LO} \cos\left(\omega_{LO} t + \phi_{LO}\right)\right]^2 \approx \\ &\approx \tfrac{1}{2}E_S^2 + \tfrac{1}{2}E_{LO}^2 + 2E_{LO}E_S \cos\left[\left(\omega_s - \omega_{LO}\right)t\right] \cos\left(\phi_s - \phi_{LO}\right)t \end{aligned} \tag{1.5}$$

where E_{LO} and E_S are the amplitude optical fields of the LO and signal, ϕ_{LO} and ϕ_S are the constant phases. Heterodyne detection is also called coherent detection since it preserves the phase of the signal. The first two terms are proportional to the average (DC) power absorbed. Note that AC contribution at the sum frequency is neglected because it's beyond the cut-off of the detector, while the interesting term is the mixing product at the beating frequency $\omega_h = \omega_s - \omega_{LO}$. The AC amplitude photocurrent generated by the detector at this frequency is proportional to the product of E_{LO} and E_S and in terms of incident power of signal (P_S) and local oscillator power (P_{LO}) is given by

$$|I_{het}| = 2\mathcal{R}\sqrt{P_{LO}P_S} \tag{1.6}$$

where $\mathcal{R}$ is the detector responsivity. The advantage of a similar technique, when the local oscillator has a much higher power with respect to the signal, is that the mixing product provides a sort of amplification of the signal, easier to detect, because the energy flux in the beating frequency is greater than the DC energy flux of the signal by itself:

$$E_{LO} > E_S \rightarrow E_S E_{LO} > E_S^2 \tag{1.7}$$

Figure 1.3 shows a schematic representation of the components involved in an heterodyne detection.

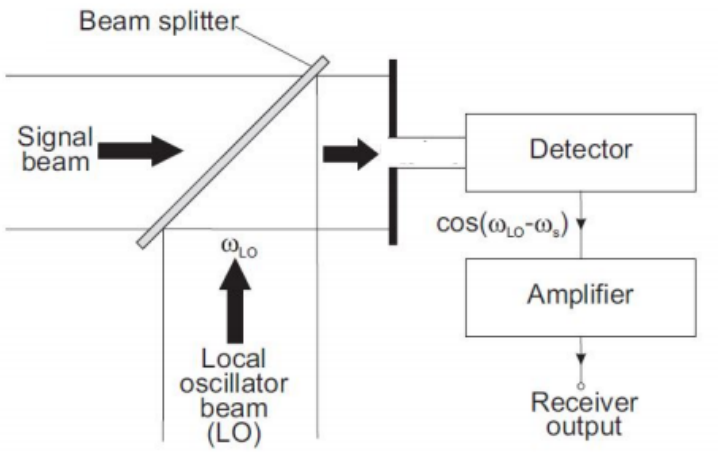

Figure 1.3: Principle of heterodyne detection based on the mixing of a signal and a local oscillator [11] by means of a beam splitter. The output is an AC signal at the beating frequency.

Part II

Experimental work

Chapter 2

Characterization of a QCD with a Mid-IR Frequency Comb

The first experiment I carried out consisted in the temporal and frequency response characterization of a 80 μm Quantum Cascade Detector fabricated by Etienne Rodriguez of *QUAD* team. In particular, in order to optimize its high-speed properties at room temperature, a specifically designed gold air-bridge structure has been realized with the shortest length possible to connect the gold contacts of the mesa (see figure 2.1 for an analogous structure of a 25 μm device): in this way the parasitic capacitance of the RC circuit is minimized leading to a smaller time constant and therefore to a larger bandwidth in frequency.

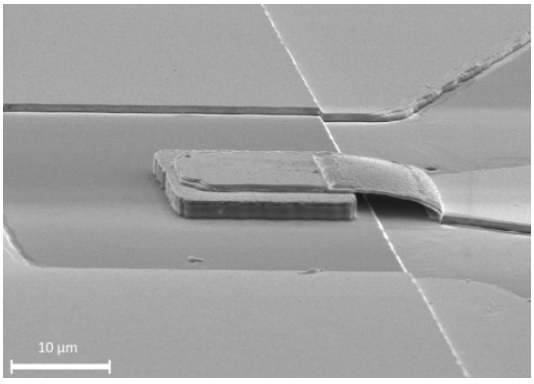

Figure 2.1: Microscope image of a 25 μm mesa with air-bridge structure. Taken from [12]

For this characterization I have been using a mid-infrared frequency comb. In this chapter I will first present the properties of the comb and then the experiment with the result of this characterization.

2.1 Principle of Frequency Combs

A frequency comb refers to a regular pulse train of a mode-locked femtosecond laser (i.e. the pulse duration is of the order of some tens of fs). In the frequency domain (i.e. Fourier space) it gives rise to a regular comb spectrum of modes with a spacing equal to the pulse repetition frequency f_{rep}, which corresponds to the inverse of the round-trip time of a pulse in the laser cavity [13].

$$f_{rep} = \frac{v_g}{L} \tag{2.1}$$

In the previous formula v_g is the group velocity of light and L the round trip length of the cavity.
In figure 2.2 a sketch of the principle of a frequency comb, adapted from [13], is shown.

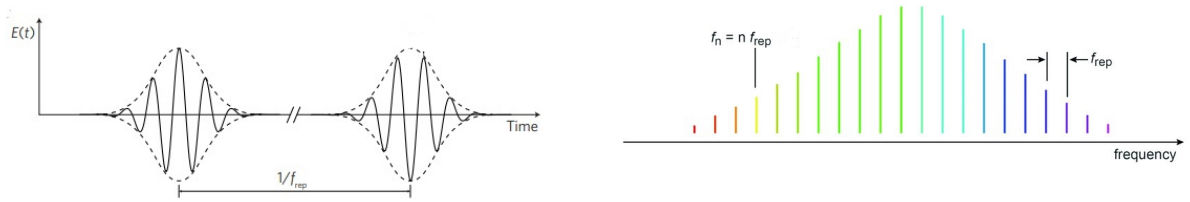

(a) Time domain pulses of the comb.The interval between each pulse is the inverse of the repetition frequency.

(b) Frequency domain spectrum of the comb. Each tooth has a frequency given by a multiple integer of f_{rep}

Figure 2.2

More specifically, I exploited a mid-IR frequency comb realized by **MenloSystems** starting from two outputs of a passively stable IR comb, respectively at 1.5 μm and 1.9 μm, that impinge on a non linear crystal and create, by Difference Frequency Generation, a mid-IR output centred at 9 μm, with a repetition frequency of 100 MHz, an optical spectrum containing more than 40000 modes and an average output power up to 2.5 mW. The result is a perfectly periodic and regular spectrum characterized by extreme stability. Providing an ultra stable reference, combs are a powerful tool in frequency metrology and their realization constituted a breakthrough in science such that their inventor, Theodor W. Hänsch, won the Nobel prize in 2005.

2.2 Temporal Pulses

The experimental setup for the QCD characterization is the following: the comb radiation is shined and focalised with a lens on the detector, which is connected to an oscilloscope. A great advantage is that QCDs structure allows to work at room T because of the absence of dark current and dark current noise, making Johnson noise the only noise mechanism in such devices [14].
Figure 2.3 shows the temporal pulses of the comb detected by the QCD, where it's already

possible to see that the interval between two pulses (i.e. the round trip time) is 10 ns and it's the inverse of the repetition frequency f_{rep} of 100 MHz.

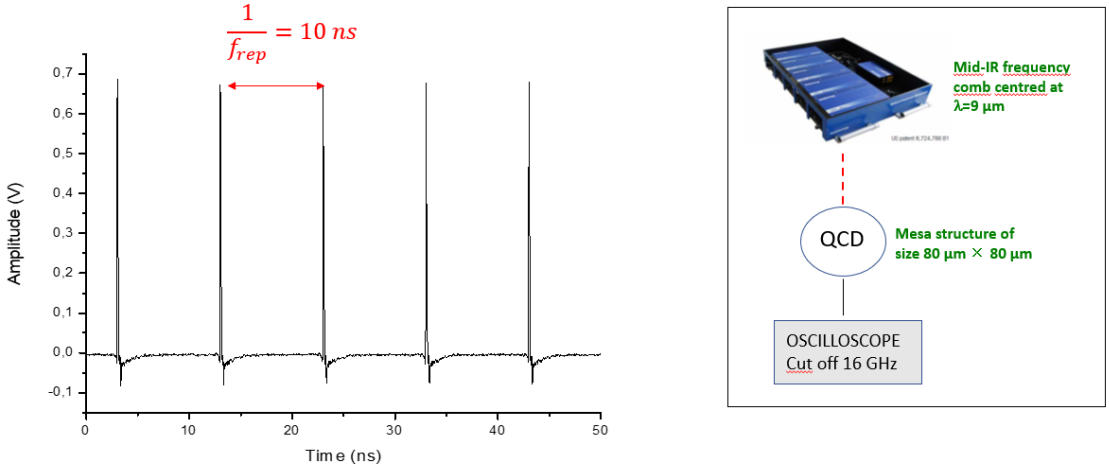

Figure 2.3: On the left: temporal pulses of the frequency comb detected by the QCD at room T. Data taken with a laser output power of 2.5 mW and a photocurrent of 1.1 μA. On the right: scheme of the setup

It is interesting at this point to study the temporal response of the QCD, by deducing, from a single pulse, the decay constant which tells us how fast the detector is in going back to equilibrium after being excited by the light, and it is strictly related to the carrier lifetime. Figure 2.4 shows on the left a exponential decay fit performed on a single pulse, which results in a decay constant of 66 ps. To understand the significant improvement in terms of time response with respect to a classical (i.e.interband) detector the right side of figure 2.4 reports a single pulse detected, in the same conditions as before, by **VIGO** detector, which shows a decay constant of 258 ps.

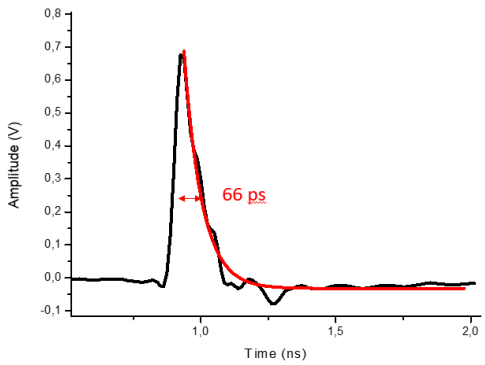

(a) Exponential decay fit on a single pulse of fig 2.3. QCD Decay constant τ = 66 ps

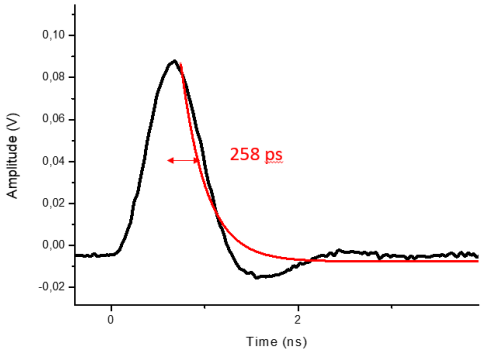

(b) VIGO impulse response. Decay constant τ = 258 ps

Figure 2.4

2.3 Frequency Spectrum

The temporal characterization already gives useful information about the frequency response of the detector. In particular, from the decay constant it's possible to deduce the cut-off frequency according to the following formula

$$f_c = \frac{1}{2\pi\tau}[\text{Hz}] \tag{2.2}$$

from which we can compute the expected values of f_c for both detectors.

Detector	τ	f_c
QCD	66 ps	2,4 GHz
VIGO	258 ps	620 MHz

By means of a spectrum analyzer connected to the detector and, exactly as before, by shining the comb laser on it, the frequency spectrum is immediately given (figure 2.5). Contrary to rectifying techniques where many measurements are necessary in order to obtain the bandwidth (a modulated voltage is applied to the detector and for each modulation frequency the resulting current is recorded), the comb allows to get it in one-shot, having per se a broad range of frequencies. Figure 2.6 shows the frequency spectrum in logarithmic scale obtained respectively with the QCD and the VIGO. One can check the bandwidth which is determined by the -3 dBm frequency and see that the QCD has a cut-off around 3 GHz while for the VIGO it's around 800 MHz, this last value being slightly different from the expected one but in agreement with VIGO datasheet.

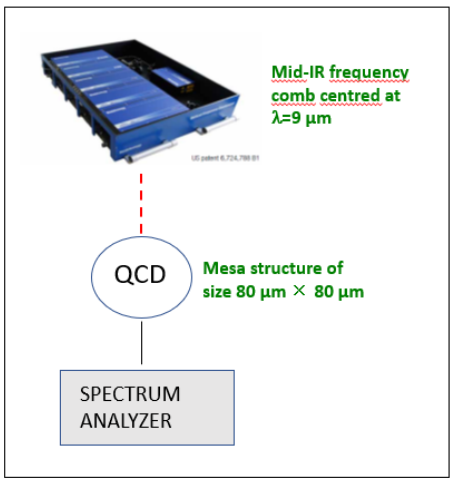

Figure 2.5: Scheme of the setup

Going more into detail, the frequency spectrum is constituted by the so called harmonics: the first harmonic is at 100 MHz because it results from the beatnote between first neighbours teeth of the comb i.e. 100 MHz distant, the second harmonic comes from all the beatings between second neighbours teeth so it's at 200 MHz and so on for the next

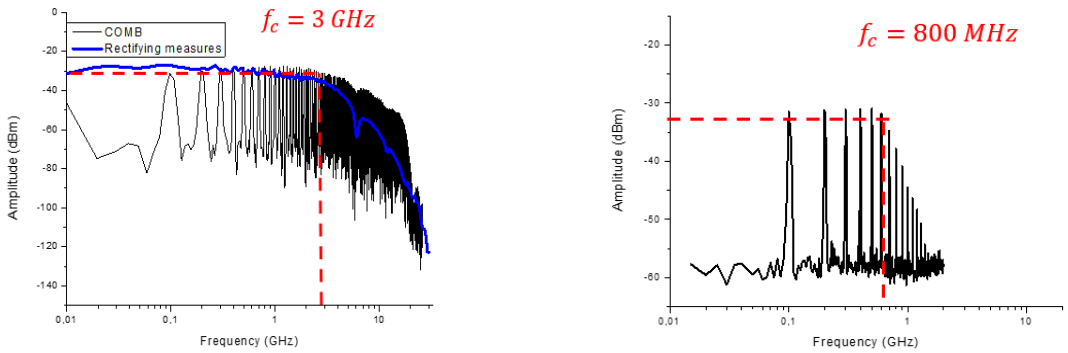

(a) QCD frequency spectrum taken with comb experiment (black) and rectifying measurements (blue): the data are in agreement.

(b) VIGO frequency spectrum. The observed bandwidth is coherent with the value on VIGO datasheet.

Figure 2.6

harmonics. In figure 2.7 the first harmonic is reported with the spectrum analyzer lowest resolution bandwidth (1 Hz): the harmonic's linewidth is extremely narrow and limited only by the instrument resolution, meaning that the teeth that are beating are highly stable so that their frequency difference is always exactly 100 MHz. This confirms the comb as an ultra stable reference, which is necessary for the experiment described in chapter 3.

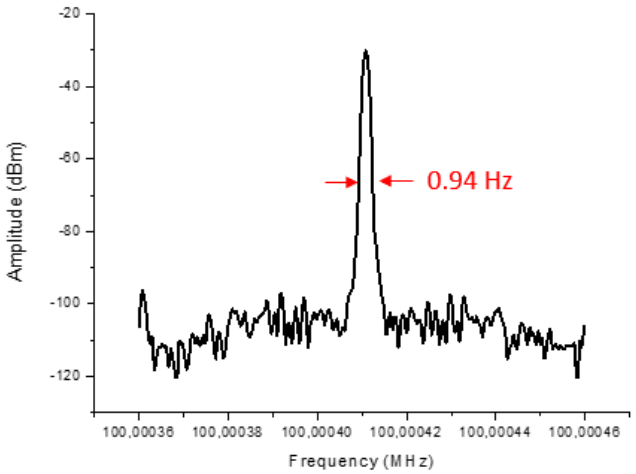

Figure 2.7: 1st harmonic of the comb. RBW = 1 Hz. Data taken with a laser output power of 2.5 mW and a photocurrent of 1.1 μA.

Chapter 3

Active stabilization of a DFB QCL on a MID-IR Frequency Comb

The stability of the frequency comb, proved by the last result of previous chapter, was exploited in the second experiment which consisted in realizing an heterodyne detection setup and actively stabilizing a distributed feedback Quantum Cascade Laser. Higher frequency stability improves the sensitivity of the system and allows implementing high-resolution techniques such as ultra-sensitive heterodyne detection. In order to do so, however, some requirements must be satisfied and it's worth to evaluate which detector, between the QCD and the VIGO, is more suited for this application.

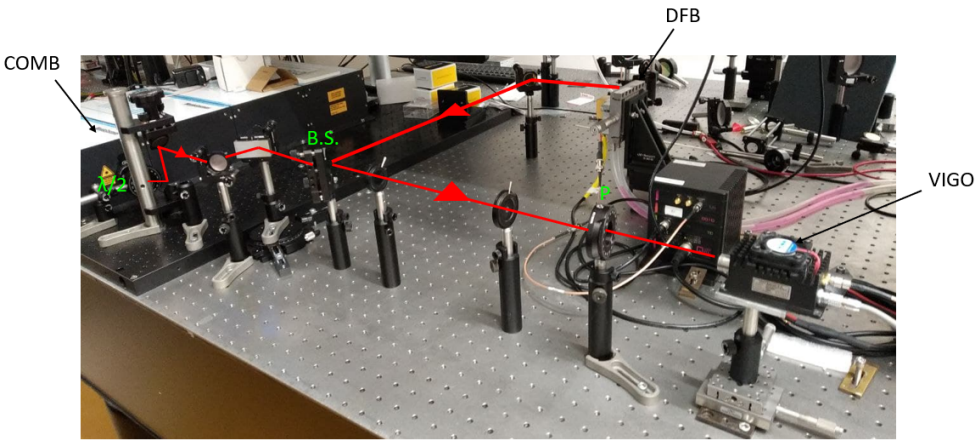

Figure 3.1: Photo of the optical part of the setup reproducing the heterodyne experiment. (BS= beam splitter, P=polarizer)

3.1 Heterodyne detection with the frequency comb

The first step for stabilizing the QCL on the comb consisted in building the setup for an heterodyne detection, whose principles have been described in paragraph 1.3. In my experiment, each individual tooth of the frequency comb constitutes a signal, while the local oscillator is provided by a single mode Distributed Feedback (DFB) QCL. In a DFB laser, a grating is implemented inside the active region and it works like a filter in frequency so as to achieve a single mode emission [15]. Figure 3.2 shows a schematic setup of heterodyne detection where, thanks to a beam splitter, the QCL mode beats with each comb tooth, and the beatings detected by the VIGO are properly amplified and sent to a spectrum analyzer, to see the frequency domain. In the same figure a graph containing the optical spectra of the QCL (in red) and the frequency comb (green) is reported: to take these measurements the comb was shined on Bristol 721 optical analyzer with an average output power of 2,5 mW, the QCL instead was set at T = 20° with a current of 290 mA . In these conditions, one can see from the graph that the comb optical emission spans from 8 to 10 μm while the DFB mode is around $9\mu m$. The DFB, however, is not stable at all due to inevitable temperature fluctuations as well as noise coming from the laser current generator: by exploiting its heterodyne with a tooth of the ultra stable frequency comb it is possible to stabilize it in frequency and phase.

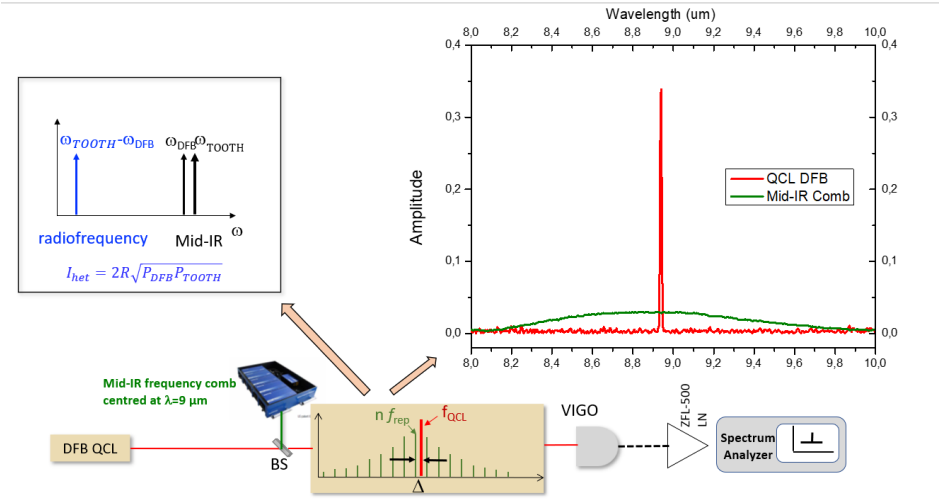

Figure 3.2: Sketch of heterodyne detection setup (BS: beam splitter, VIGO: detector, ZFL-500 LN: low noise amplifier). Right inset: optical spectra of QCL (red) and comb (green) taken with Bristol 721 analyzer. Left inset: range of frequencies interested by the heterodyne effect.

The first observation of the heterodyne beatnotes is shown in figure 3.3, where it's possible to compare them with the harmonics of the comb: the difference in the amplitude comes from the fact that the harmonics contain the beatings of multiple teeth with each other, while for the heterodyne it's just one tooth beating with the DFB. The scheme in the right side of 3.3 explains what we see on the left: the QCL is around 20 MHz distant from the closest tooth of the comb and 80 MHz distant from the second nearest one, so the first beatnote will be seen at 20 MHz, the second one at 80 MHz. Similarly, after the

first harmonic at 100 MHz (which we remind is the repetition frequency of the comb, see chapter 2.2), there are the signals corresponding to the beating of the QCL with the teeth distant respectively 120 MHz and 180 MHz, and so on for the next ones.

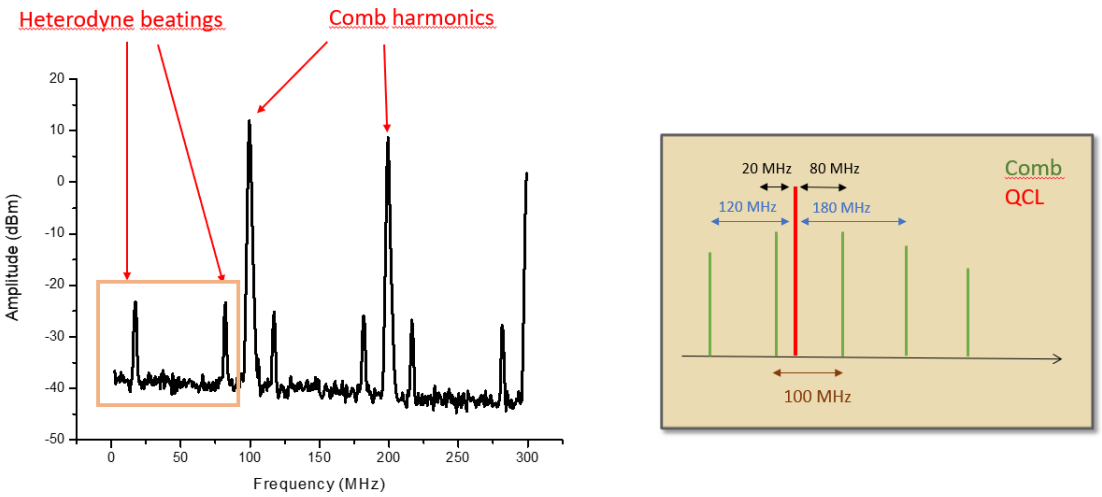

Figure 3.3: First observation of heterodyne beatings in frequency domain. RBW = 1MHz. Data taken with the following parameters: comb output power = 2,1 mW, DFB current setpoint = 312 mA, DFB Temperature = 20°C, Amplifier ZFL 500 LN.

The DFB instability can be observed indirectly by looking at the linewidth of the beatnote: the comb mode, in fact, is ultra stable and comparable to a delta, so the broadening is caused entirely by the frequency fluctuations of the DFB. Figure 3.4 shows a single beating at a resolution bandwidth of 10 kHz, which allowed to perform a gaussian fit and obtain a FWHM of 0.5 MHz.

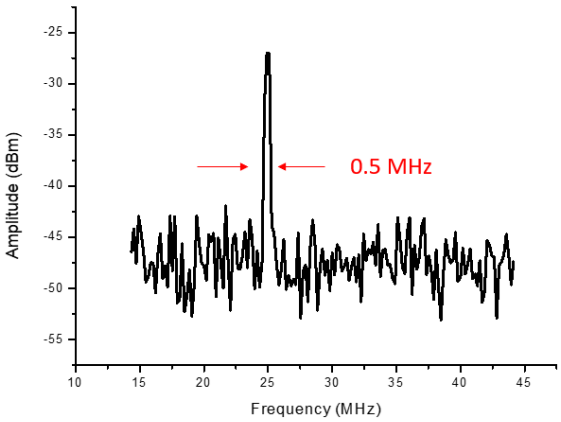

Figure 3.4: Single beating at RBW = 10 kHz. Data taken with the following parameters: comb output power = 2,1 mW, DFB current setpoint = 312 mA, DFB Temperature = 20°C, Amplifier ZFL 500 LN

3.2 Active stabilization of the DFB laser: conception of the experiment

The active stabilization of the DFB is performed by means of the phase lock technique, which allows to stabilize a signal in frequency and phase by comparing it with a reference signal and generating a current proportional to the difference between the two, which is sent as a feedback to the unstable source to correct it. In this paragraph I will discuss why I decided to use the VIGO detector instead of the much faster QCD in the stabilization experiment. Nonetheless it must be said that the QCD is equally suitable for the detection of the heterodyne alone ([16]).
In order to lock a signal, it is necessary for it to have at least 0dBm of power and to have the highest possible signal to noise ratio (SNR). It is interesting, to this purpose, to calculate the expected power associated to beating level and noise level both in the case we use a QCD and a VIGO: in fact, besides the different physical mechanism, they have really different characteristics in terms of responsivity and noise contributions.
As far as the VIGO is concerned, the power associated to the noise is computed taking into account the preamplifier integrated in the detector, according to the scheme in figure 3.5. The detector is modeled by a photocurrent source i_{ph} , shunt resistance R_d and capacitance C_d, while the transimpedance amplifier is an operational amplifier with feedback resistance R_f and capacitance C_f. Since the heterodyne occurs at low frequencies all capacitances are equivalent to open circuits.

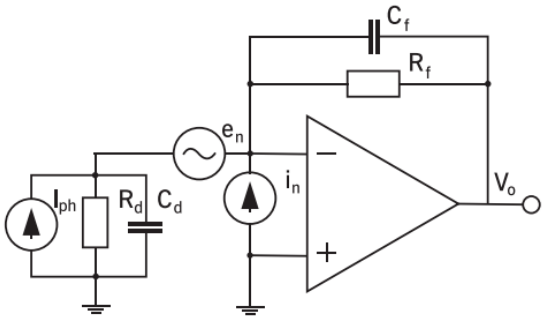

Figure 3.5: Transimpedance circuit of VIGO taken from its datasheet.

As follows from the transimpedance circuit, the preamplifier current noise at low frequencies is approximated as:

$$i_{pa}^2 = \frac{4k_bT\Delta f}{R_f} + i_n^2\Delta f + \frac{e_n^2\Delta f}{R_d^2} \tag{3.1}$$

where the first term is thermal noise on the feedback resistance, the second is the open input current noise and the third one comes from the short input voltage noise. To this noise, one has to add also the dark current (i_d) shot noise, given by

$$i_{n,d}^2 = 2i_d e\Delta f \tag{3.2}$$

where e is the electron fundamental charge and Δf the resolution bandwidth. Finally, when the detector is illuminated the photocurrent shot noise is present too

$$i_{n,ph}^2 = 2i_{ph}e\Delta f \tag{3.3}$$

where the photocurrent is given by heterodyne formula 1.6.
As for the QCD, it can be modeled by a simple resistance R_d in which the main contribution to the noise is given by the thermal noise on R_d, while dark current shot noise and photocurrent shot noise play a negligible role. The power associated to the noise is finally obtained by multiplying the total current noise by the load resistance of the spectrum analyzer R_L = 50Ω.
The power associated to the beating is computed starting from the heterodyne photocurrent of formula 1.6 and multiplying its square modulus by R_L. The chosen values for P_{LO} and P_S are different in the two detectors: the VIGO, in particular, saturates when the total incident power on its surface is overcoming 200 μW. Assuming P_{LO} =100 μW coming from the DFB and 100 μW coming from the comb, by computing its exact number of teeth its possible to get the power of a single tooth P_S, equal to 2,33 nW. The number of teeth is deduced by taking the frequency equivalent of the envelope spectrum in figure 3.2 and dividing its FWHM by the repetition rate of the comb :
$f_{rep} = 100MHz$
FWHM of the envelope spectrum = $4,29 * 10^{12} Hz$

$$\#\text{ modes } = \frac{4.29 * 10^{12}}{100 * 10^6} = 42900 \tag{3.4}$$

The QCD doesn't have saturation problems so we can assume much higher powers like P_{LO} = 20 mW from the DFB and a total power from the comb of 300 μW, that gives a P_S of 6,99 nW. In addition to that, the QCD doesn't have the preamplifier inside so, in order to fairly compare the two detectors, we can imagine to add to it an amplifying stage with the same transimpedance gain of VIGO, $R_f = 8,65m\Omega$, for which the photocurrent is multiplied. In this way, the performances of the two detectors will be only influenced by the difference in responsivity $\mathcal{R}$: the VIGO has a responsivity of 3 A/W (given by datasheet) while for the QCD a responsivity of 5 mA/W has been deduced from the slope of the photocurrent vs incident power measurements. Table 3.1 contains the values of beating signal and noise floor (at RBW = 1MHz) for VIGO, QCD, and amplified QCD : comparing the first and third line, we can see that even if we add a transimpedance gain to the QCD the beating has a too low level (-46,80 dBm) to be suitable for active stabilization. The signal obtained with the VIGO is three orders of magnitude higher (-19,03 dBm), allowing to reach 0 dBm with few amplifiers, while for the QCD a larger number of further amplifiers would be necessary, certainly incurring their saturation and therefore affecting their gain. In conclusion, QCD responsivity at room temperature is not enough to allow the phase lock of the signal, so VIGO must be used. The drawback of VIGO is however the saturation, that is, the decrease of its responsivity when the incident power is too high. The signal-to-noise ratio of the beatnote in figure 3.3 is only 15 dBm and, in fact, it is largely affected by the detector saturation. Nevertheless it didn't constitute a problem for the active stabilization, whose setup is described in the next paragraph.

Table 3.1: Comparison of VIGO and QCD in terms of signal and noise levels

Detector	$\mathcal{R}$ (A/W)	P_s (W)	P_{LO} (W)	R_f Ω	beating (dBm)	noise (dBm)
VIGO	3	$2,33 \times 10^{-9}$	100×10^{-6}	$8,65 \times 10^{-3}$	-19,03	-76,65
QCD	5×10^{-3}	$6,99 \times 10^{-9}$	20×10^{-3}	/	-91,55	-110
QCD + pre amp	5×10^{-3}	$6,99 \times 10^{-9}$	20×10^{-3}	$8,65 \times 10^{-3}$	-46,80	-76,65

3.3 Phase Lock

The experimental setup for the active stabilization is schematically represented in figure 3.6. The comb and DFB radiations are combined through a beam splitter and sent to the VIGO (note that the alignment of the two beams on the detector is not straightforward because the two beams are in the infrared). From the VIGO the electrical signal is splitted: one part (input B) goes to the spectrum analyzer allowing to see the beatings just as in figure 3.3, the other part (input A) is filtered by a low pass 50 MHz filter and a narrower band pass 19-23 MHz filter (in fact, we're interested in just one beatnote) and then amplified with two amplifying stages in order to arrive to the Phase Lock Loop (PLL) with ≥ 0 dBm. The PLL is the component effectively performing the stabilization: it is connected to a RF generator to compare the two signals it receives in input, and its output is a correction signal for the DFB. When the lock is successful one can check it on an oscilloscope that receives the AC and DC error between the two signals: if they're both constant and close to zero the signal has been corrected. As the comb and DFB have respectively horizontal and vertical polarization, a $\lambda/2$ plate is present at the output of the comb to adjust it : the $\lambda/2$ is wavelength-specific so it actually turns the polarization of the comb modes that are in an interval around 9 μm. All the other modes will not generate the heterodyne beating, and are properly filtered by means of a polarizer to reduce the optical 'useless' power impinging on the VIGO that would only contribute to its saturation. To the same purpose of reducing the detector saturation, a reflective diffraction grating replaces one of the mirrors that deflect the comb beam: the 1st reflection order, in fact, will spatially separate different λ components so that only a fraction will meet the beam splitter and participate to the heterodyne.

After a successful phase lock, we are able to observe the signal at 1 Hz of resolution bandwidth because we achieve the desired stability. The result is shown in figure 3.7. Such a result is of great importance not only for the achieved stabilization of the QCL, but also for the Noise Equivalent Power (NEP) of the heterodyne detection: from the signal to noise ratio we see that 65 dBm of power are concentrated in 1 Hz, so that in principle the signal P_S can be up to six order of magnitude lower and we would still be able to detect it (looking at the P_S values in the order of the nW in table 3.1, this would mean achieving a NEP of some fW) . This is clearly a fundamental step towards the ultra-sensitive heterodyne detection.

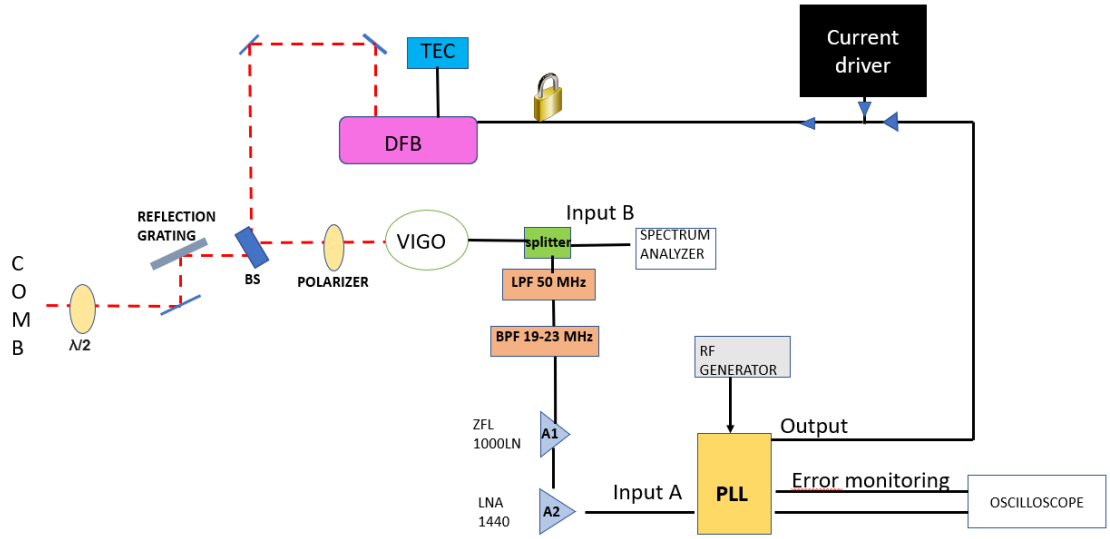

Figure 3.6: Scheme of the experimental setup for the the active stabilization. Legend: BS = beam splitter, TEC = temperature controller, LPF = low pass filter, BPF = band pass filter, ZFL 1000 LN and LNA 1440 = low noise amplifiers, PLL = Phase Lock Loop.

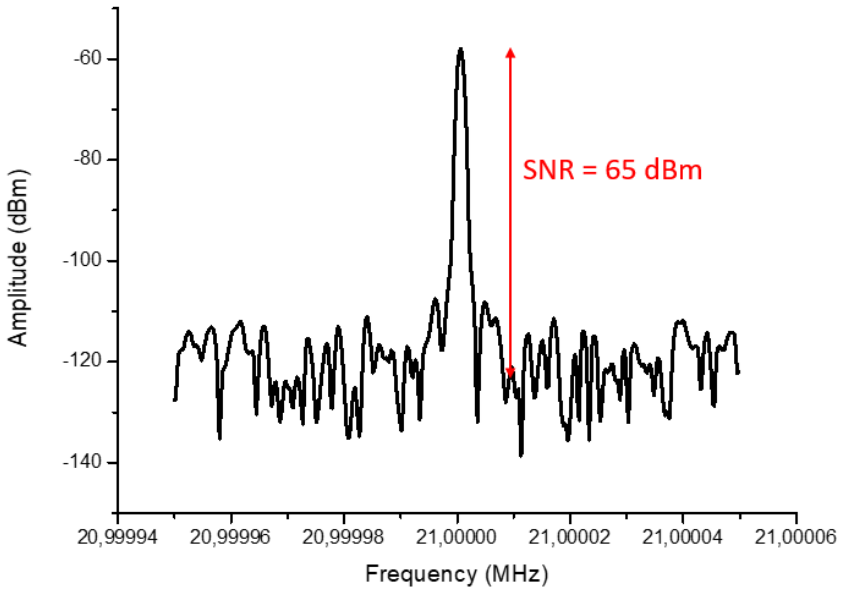

Figure 3.7: Locked signal at input B. RBW = 1 Hz.

Conclusion

My internship activity evolved around the innovative frequency comb present in the laboratory. First, it allowed the characterization of the Quantum Cascade Detector, and finally it was exploited as an ultra stable reference for phase locking a Quantum Cascade Laser. My training was mainly focused on setting up from scratch these two experiments, finding good alignment conditions and learning to work with the lasers and detectors, but it also included a more theoretical part about the study of noise and signal of the heterodyne beating, relevant for evaluating which detector ensured the best conditions for the phase lock. Building successfully the setup for the heterodyne detection constituted one of the most challenging parts, due to the alignment of the different optical components in the mid-infrared: in order for the two beams to combine effectively after the beam splitter, they have to overlap throughout all the optical path and not only on the surface of the detector. Achieving a successful and stable phase lock was another challenging point due to the delicate electronic components inside the Phase Lock Loop, so that a lot of attention was paid in order to create the optimal conditions for the PLL to work: for instance, reducing the VIGO saturation to obtain a higher SNR was a concern, so that the polarizer was introduced. The next step is, to this purpose, tilting the reflective diffraction grating, which was so far used as a mirror, to exploit its first order of reflection.
As a future perspective, the active stabilization of the QCL allows realizing a very good local oscillator for remote sensing applications (LIDAR) or for pushing the detection capability down to the single photon limit.

Bibliography

[1] John Nelson Howard and John Seymour Garing. "The transmission of the atmosphere in the infrared—A review". In: *Infrared Physics* (1962).

[2] S. Blaser et al. "Free-space optical data link using Peltier cooled quantum cascade laser". In: *Electronics Letters* 37 (2001).

[3] P. Geiser et al. "A subnanosecond pulsed laser-source for mid-infrared LIDAR". In: *Applied Pysics B - Laser and Optics* 83 (2006), pp. 175–179.

[4] H. Schneider and H. C. Liu. "Quantum Well Infrared Photodetectors: Physics and Applications". In: *Springer Series in Optical Sciences* 126 (2007).

[5] "Quantum cascade detectors: A review". In: *Mid-infrared Optoelectronics*. Ed. by Eric Tournié and Laurent Cerutti. Woodhead Publishing, 2020, pp. 337–377.

[6] Azzurra Bigioli. *Uncooled unipolar receivers for 9 µm wavelength heterodyne detection*. PhD Thesis, 2021.

[7] L.Li P. Bai et al. "Optical field simulation of edge coupled terahertz quantum well photodetectors". In: *AIP Advances* 8 (2018), p. 035214.

[8] Ronsencher and Vinter. *Optoelectronics*. Cambridge University Press, 2002.

[9] Dougakiuchi et al. "Ultimate response time in mid-infrared highspeed low-noise quantum cascade detectors". In: *Applied Physics Letter* 118 (2021).

[10] M. Teich. "Infrared heterodyne detection". In: *Procedings of the IEEE* (1968).

[11] A Rogalski. *Infrared and Terahertz Detectors*. CRC Press, 2019.

[12] Etienne Rodriguez et al. "Room-Temperature, Wide-Band, Quantum Well Infrared Photodetector for Microwave Optical Links at 4.9 μm Wavelength". In: *ACS Photonics* 5 (2018), pp. 3689–3694.

[13] Albert Schliesser, Nathalie Picqué, and Theodor W. Hänsch. "Mid-infrared frequency combs". In: *Nature photonics* (2012).

[14] Xuejiao et al. "Room temperature quantum cascade detector operating at 4.3 um". In: *Journal of Semiconductors* 35 (2014).

[15] Angela Vasanelli and Carlo Sirtori. *Lasers à cascade quantique*. Techniques de l'Ingénieur, 2019.

[16] Azzurra Bigioli et al. "Long-wavelength infrared photovoltaic heterodyne receivers using patch-antenna quantum cascade detectors". In: *Applied Physics Letters* 116.16 (2020), p. 161101.